ENERGETIC PARTICLE EXPERIMENT ERNE

J. TORSTI, E. VALTONEN, M. LUMME, P. PELTONEN,
T. ERONEN, M. LOUHOLA, E. RIIHONEN, G. SCHULTZ, M. TEITTINEN
Space Research Laboratory, University of Turku, FIN-20520 Turku, Finland
K. AHOLA, C. HOLMLUND, V. KELHÄ
VTT Automation, Space Technology, FIN-02044 VTT, Finland
K. LEPPÄLÄ, P. RUUSKA, E. STRÖMMER
VTT Electronics, Box 1100, FIN-90571 Oulu, Finland

Abstract. The Energetic and Relativistic Nuclei and Electron (ERNE) experiment will investigate the solar atmosphere and the heliosphere by detecting particles produced in various kinds of energy release processes. ERNE is at the upper end in energy among the SOHO particle instruments. The instrument will measure the energy spectra of elements in the range Z=1–30. The energy coverage varies dependent on the particle species from a few MeV/n up to a few hundred MeV/n and electrons from 2 to 50 MeV. At high energies, ERNE records also the direction of the incident particles for accurate measurements of the pitch angle distribution of the ambient flux within the viewing cone. Especially the isotope identification capability has been one of the instrument design goals, thus providing new data regarding various fundamental questions in solar physics.

Key words: solar physics – cosmic rays – solar flares – coronal mass ejections

1. Introduction

ERNE measures energetic particles: electrons, protons and isotopes of heavier elements. It measures the energies, identifies the particles and records the directional distribution of the flux of solar particles. The research program of ERNE and the SOHO satellite is to understand the structure and behavior of the Sun, and to investigate the open questions related to the cosmic ray modulations in the solar system.

The two-year measurement period starting at the end of 1995 coincides with solar activity minimum, when the low noise level of the interplanetary magnetic field (IMF) allows observation even of minor events.

Among the most important problems still lacking a sufficient answer are the mechanisms of energy release and transport, the chemical and isotopic composition in different parts of the solar atmosphere, the processes of particle acceleration, magnetic field reconnection on various spatial and temporal scales, the generation and properties of different types of shocks, relations between various phenomena occuring in active regions (e.g., flares, coronal mass ejections, erupting filaments, shocks), and the propagation of energetic particles in the IMF and the extent of interplanetary acceleration. Key contributions towards solving these problems can be obtained from suprathermal and energetic particle observations by using these particles as diagnostic

Solar Physics **162**: 505–531, 1995.

tools for remote probing of solar processes. Most of these processes have a distinctive signature in the timing, composition, and energy spectra of the accelerated particles.

Being outside the Earth's magnetosphere, the particle instruments on board SOHO have a direct view of the charged particle flux coming along the interplanetary magnetic field line.

Measurement of energy spectra of various ions as well as isotopic abundance ratios gives information on the acceleration of solar energetic particles. By adding measurement of the anisotropy of the particle flux at the spacecraft location, it is possible also to study the propagation of these particles in the IMF.

The measurements will cover particle flux at quiet time, solar particle events, flux enhancement due to particle acceleration by interplanetary shocks and solar modulation of galactic cosmic rays.

This experiment supported by the other particle and solar wind experiments on board SOHO will give a detailed picture consisting of various particle types and energy ranges. Together with observations of other instruments of the SOHO mission this will form a database for research of solar phenomena in detail - particle observations can be related to observed characteristics of the region where particles are accelerated. Because no local magnetic field measurements are carried out on board SOHO, collaborative work with other spacecrafts producing magnetic field data is needed.

At an early phase of SOHO project, ERNE and COSTEP (Comprehensive Suprathermal and Energetic Particle Analyzer) (Müller-Mellin et al., 1995) formed a collaboration called CEPAC (COSTEP-ERNE Particle Analyser Collaboration). Although ERNE and COSTEP are separate investigations, their instruments have been adjusted to each other so that a wide range of particle energies and species from the energetic heavy nuclei to suprathermal electrons is covered.

CEPAC consists of three sensor units, which have common interfaces to the spacecraft data handling system through the Common Data Processing Unit (CDPU) and to the spacecraft power bus through the Low Voltage Power Converter (LVPC).

Design and production of the ERNE Sensor Unit (ESU), LVPC and CEPAC common ground support equipment were responsibilities of the ERNE part of CEPAC.

2. Scientific Objectives

2.1. Solar particle production

Impulsive solar particle events originate in compact regions low in the corona. These events are characterized by a large number of electrons compared to protons. Impulsive events with enriched ^{3}He and heavy element popu-

lations are particularly interesting, because they may provide the purest signature of impulsive acceleration processes.

Many energetic particle events seem to be associated with large coronal mass ejections, CME-events (Gosling, 1993). The CME-related shock fronts cause particle acceleration and in fact seem to be responsible for producing the large, gradual SEP events.

The westward location of a solar flare on the Sun leads to a fast rising flux of prompt flare particles, due to the connecting magnetic field lines. Also, it is well known that energetic solar particle event observations from the western hemisphere are more frequent than from the eastern part. Somewhat surprising, an annular area with angular distance of more than 20° from the exact footpoint of the magnetic field line connecting to Earth seems to be more effective in producing energetic particle events observable close to Earth than the footpoint region itself (Torsti et al., 1994).

Solar particle events originating at various locations and related to different processes have characteristics distinguishable from each other. With ERNE, the combination of a large geometric factor, good time resolution and simultaneous measurements of electrons, protons, and heavier ions and their energy spectra over a wide range will give new contributions to the characterization of various kinds of SEP events and to the determination of the properties and environment of the source regions. Energetic particles can make contributions towards the identification of the mechanisms for heating the corona, for accelerating the solar wind, and for transporting matter up from the photosphere. Microflares responsible for coronal heating can also result in energetic electron and ion emission.

2.2. Particle Flux Composition

Energetic particle emissions carry information about the solar atmosphere because fast particles such as 1 MeV protons are truly collisionless – they are free to move in the coronal magnetic structures. Hard collisions, although rare, are responsible for nuclear fragmentation and the release of energetic neutrons, which have free escape even from layers deep in the solar atmosphere.

The photospheric plasma is not highly ionized, there are a lot of neutral and singly ionized elements present. This means that for each element the ion/neutral ratio depends on the atomic first ionization potential (FIP) of that element. The abundances in the outer solar atmosphere differ from photospheric values. The abundances of corona, solar wind and SEP show a dependence on FIP. This is clearly seen in gradual SEP events and is less pronounced in an impulsive event where hotter plasma is involved. The SEP abundance of low FIP elements (below 9 eV) is about 4 times higher than the photospheric values. High FIP elements (above 11 eV) show the same

abundances in SEP and photospheric values with the exception of the very high FIP He (24.5 eV) which is suppressed (Reames 1995).

Isotopic composition of SEP is a path for obtaining the isotopic composition of the solar atmosphere, which cannot be obtained by spectroscopic observations. Isotopic composition of SEPs will give new insights into the origin and evolution of the solar system as well as give additional valuable information about the acceleration and injection of SEPs and about the transport of photospheric heavy ions into the corona.

Within the resolution and geometrical factor of ERNE we expect to be able to determine the variation of He isotopes as a function of time and to determine the deuteron to proton ratio as well as ratios of the less abundant isotopes of, e.g., carbon, nitrogen, oxygen, neon and magnesium.

The direct determination of the elemental and isotopic compositions of the solar atmosphere at different sites is one of the main goals for ERNE. The measurements will add new species to the known abundances. The elemental composition of solar energetic particles is measured in long duration flares which sample large coronal regions, and in impulsive flares which sample small, hot sites, rich in heavy ions.

2.3. Particle Acceleration

There are at least four distinct energetic particle acceleration processes suggested to operate in the solar atmosphere: impulsive acceleration in reconnection electric fields related to the flash phase of a flare; stochastic acceleration in turbulent regions after a flare; low coronal shock acceleration immediately after the impulsive phase; and the acceleration in high coronal shocks associated with the largest flare events and CMEs (for a review see, e.g., Forman et al., 1986). These different processes operate at different coronal sites with the result that distinct energetic particle signatures are created.

A clue to the acceleration mechanism might come from the selective acceleration of heavy elements. It is known (Schwenn and Marsch, 1990) that the helium to proton ratio in the solar wind is greater (3.6%) in the fast wind than in the slow wind (2.5%).

The ratio of ^{3}He to ^{4}He, and in general, the isotope separation provided by ERNE is a quantity carrying information of the acceleration mechanism at work. A turbulent spectrum of waves will give a Fermi-type particle acceleration, while discrete waves will be q/m and energy-sensitive. Our dual method of taking a raw sample of the flux, and additionally packing protons and helium data giving priority to the rare heavy elements for the rest of the data package, is designed to maximize the physics information. The ERNE measurements are to be supplemented by microwave radio measurements of the source regions at the Sun.

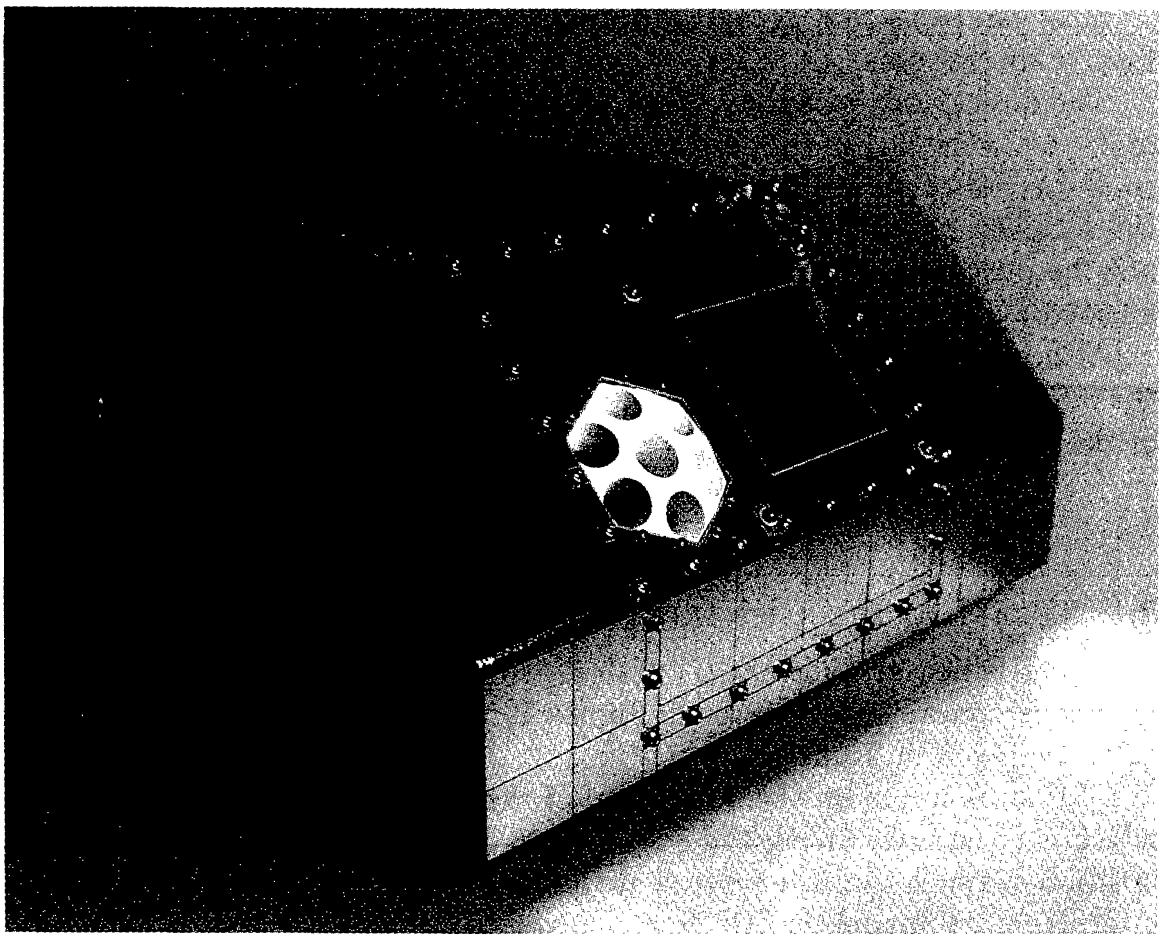

Fig. 1. ERNE Sensor Unit.

2.4. Coronal injection and interplanetary transport

Time-intensity and time-anisotropy profiles contain information on the acceleration and release processes of the Sun as well as on the interplanetary medium (Wibberenz et al., 1989, Kunow et al., 1991).

Suprathermal and energetic particle observations outside the Earth's magnetosphere near 1 AU can be used to study in situ the process of particle acceleration by interplanetary shocks as they travel out from the Sun. The continuous energy coverage enables the identification of the "seed population", i.e., particles could be pre-accelerated in some non-shock related process.

The CME shocks are driven by clouds of gas travelling outwards. In addition, there are tangential shocks. The fast wind is connected with magnetically open regions of the Sun (coronal holes), while the slow wind originates from magnetically closed regions (arcs). When the fast wind corresponding to a loose spiral runs into the slow wind on a tight spiral, a complicated

shock pattern results, which can both accelerate particles and show up as turbulence.

Solar neutrons that decay to protons on the field line connecting to Earth form a special case.

The directional resolution of ERNE within the viewing cone is of the order of 1°, whereas earlier spinning satellites could only provide us with typical resolution of the order of 45°. When a shock front, e.g., after a CME, passes the satellite, the direction of the magnetic field line changes rapidly. It will now be possible to get the temporal structure of the related changes in the anisotropy.

Although no direct measurement of the magnetic field is done by SOHO, the measured pitch angle distribution can be used to determine the direction of the field line.

3. Instrument Description

3.1. Technical specifications

The ERNE Sensor Unit (ESU) with its two sensors and all associated electronics is contained in one box (Figure 1). Main physical characteristics of ESU are given in Table I.

ESU is mounted on the + X panel of the SOHO payload module (PLM), which is constantly facing the Sun. Design of the ESU box and its mounting position are such that the sensors are looking into the direction of the average interplanetary magnetic field line.

TABLE I

Main physical characteristics of ESU

Dimensions (LxWxH) (mm)	
Main box envelope	382 x 185 x 163
Radiator width	340
Box structural material	2618 A-T652 Al alloy
Mass (kg)	9.305
Mounting	PLM + X face, - Y edge; hard mounted on 6 lugs
Field of view (half angle)	
LED	32°, circular
HED	60°, rectangular
Boresight direction	Azimuth 180°, elevation 45°
Alignment	± 2°

ESU is a thermally individually controlled unit. It is mounted on six thermal washers designed to minimize conducted heat flux between the unit and the PLM. All surfaces inside the cavity formed by the PLM roof and

spacecraft thermal blanket are covered with low emissivity aluminized kapton tape. The radiator surface in front of ESU (see Figure 1), having an almost unobstructed view to empty space, is covered with an optical solar reflector. The purpose of this surface is to provide cooling by minimizing the absorbed heat flux and maximizing the emitted flux. Active control of the ESU temperature is achieved by software-driven operational heaters.

ESU has two electrical interfaces to the other CEPAC units. One is for data and electronics power with the CDPU and the other one with the LVPC for non-operational and operational heater power.

All electronics supply voltages from the LVPC are distributed to the ESU through the CDPU, allowing the CDPU to switch the ESU on and off. The power consumption of the ESU in different operational modes is given in Table II.

The data interface between the CDPU and the ESU is a 9600 baud asynchronous bi-directional serial link. In addition to nominal and redundant data lines, a timing signal and the monitoring of spacecraft powered thermistors are directed through this interface.

3.2. Operational characteristics

To achieve the scientific goals of ERNE, ESU has two sensors and low noise electronics with a wide dynamic range.

Both sensors have a telescopic structure. In the Low Energy Detector (LED), semiconductor detectors are used. The High Energy Detector (HED) employs scintillators in addition to semiconductor detectors. Together the two sensors cover the energy range from 1 MeV/n up to hundreds of MeV/n and ions from hydrogen to zinc. Electron flux is determined in the energy range 2 to 50 MeV. Details of the energy coverage for some ions are shown in Figure 2. Expected capability of isotope identification of the elements is also indicated.

In order to be able to measure the abundances of rare elements and isotopes, the large geometric factor of the sensors is essential, particularly at high energies. HED has an energy dependent geometric factor as presented in Figure 3. Typically, for ions the geometric factor varies between 25 – 40 cm^2sr. This allows abundances of several elements and isotopes to be measured, which are not known today or are known only with modest accuracy. Due to different event triggering conditions, the acceptance of electrons has different characteristics and varies between 13 – 60 cm^2sr. Geometric factor at the lowest energies is 0.26 cm^2sr (LED I) and at medium energies 0.64 cm^2sr (LED II) (for definition of LED I and LED II, see Section 3.3.1).

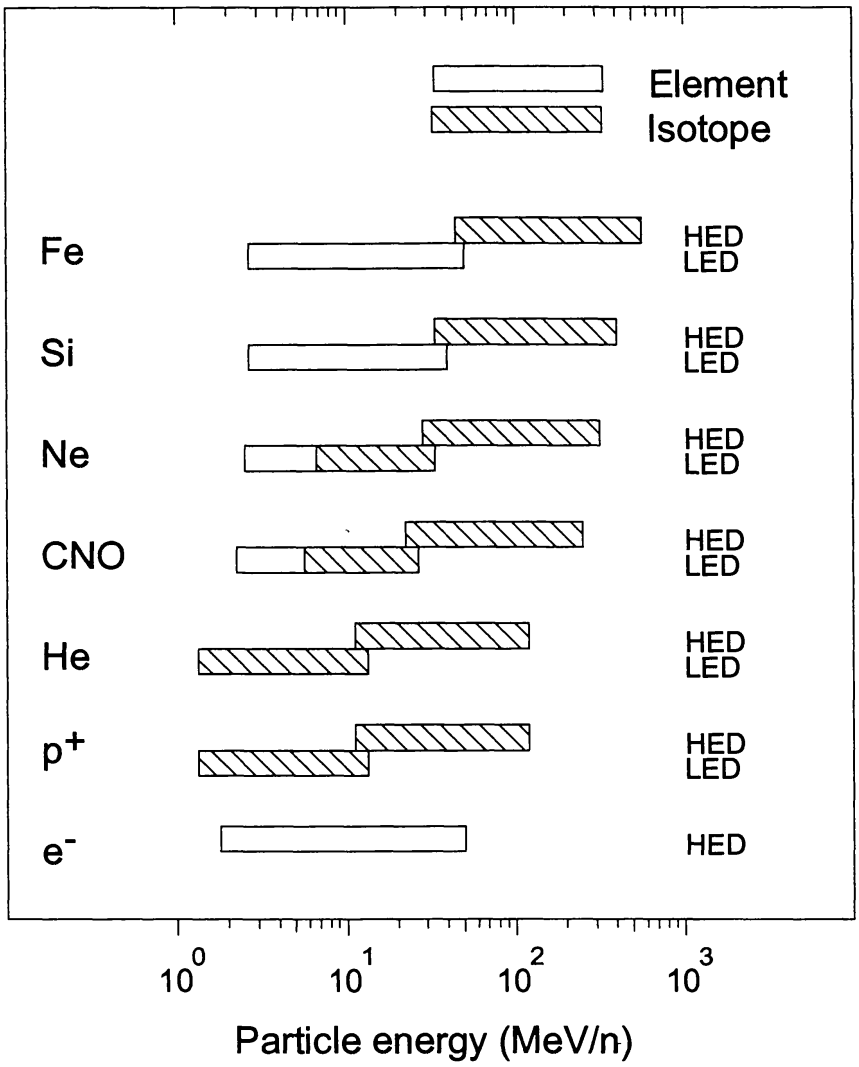

Fig. 2. ERNE measurement ranges.

The bit rate allocated for ESU is 768 bits/s. This sets quite severe limits on the amount of data that can be transferred to Earth. Therefore, the most abundant ions are analyzed on-board (see Section 3.6) to minimize the down link of raw data. For the same reason, the basic time resolution of the instrument is one minute (more precisely 59.953 seconds). However, both ESU sensors have counters giving count rates of protons every 10 seconds.

ESU has several operational modes as presented in Table II. The upload mode is used to read programs and data from the PROM memory to the RAM area at switch-on of the ESU data processing unit. The duration of this mode is only 50 ms. Standby is the safe mode of the ESU. The purpose of the maintenance mode is to allow various pre-defined contingency operations to be performed in case need arises.

The operational scenario during the flight is very simple. After initial commissioning, which includes checking of all functions of the electronics and

the performance of the sensors, ESU is switched into the nominal observation mode (ON mode). This mode will be maintained during the entire mission, with exceptions of regular transitions into the calibration mode and back about once in a month. In case of failures, one of the several backup modes can be used. The ESU hardware is then operated in a reconfigured mode, to allow elimination and by-pass of failed parts.

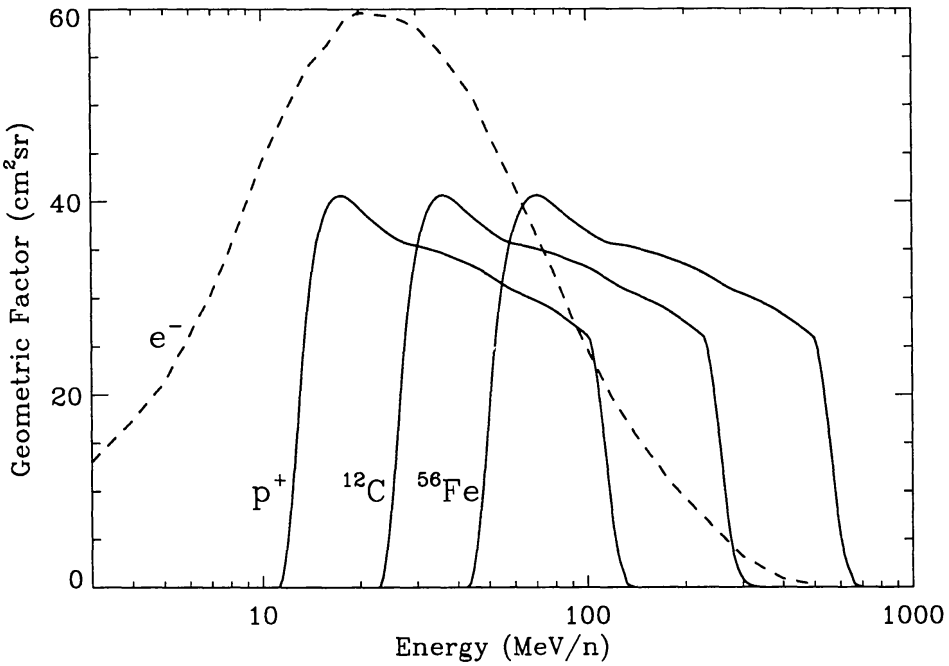

Fig. 3. The geometric factor of HED as a function of energy for electrons and three ions. The dashed electron curve is the result of simulation, the solid ion curves are calculated from theoretical range formulae and the HED geometry.

TABLE II

Operational modes of ESU

Mode	Description	Power (W)
OFF	All power off.	0.0
UPLOAD	Program upload. PROM on.	3.0
STANDBY	DPU on. LED bias on.	1.7
MAINTENANCE	Test or reconfiguration of HW.	min. 1.7, max. 7.1
ON	Nominal observation mode.	6.8
CALIBRATE	Calibration mode.	7.1
BACKUP	HW reconfigured.	min. 3.8, max. 6.8

3.3. Design principles of sensors

3.3.1. Low Energy Detector

LED consists of two layers of silicon detectors used for energy measurements followed by a third detector operated in anticoincidence with the upper two layers (Figure 4). The anticoincidence detector is used to veto against particles penetrating through the entire sensor. The pulse height data of these penetrating particles are not analyzed, but the integral flux of all such particles is recorded in one counter channel.

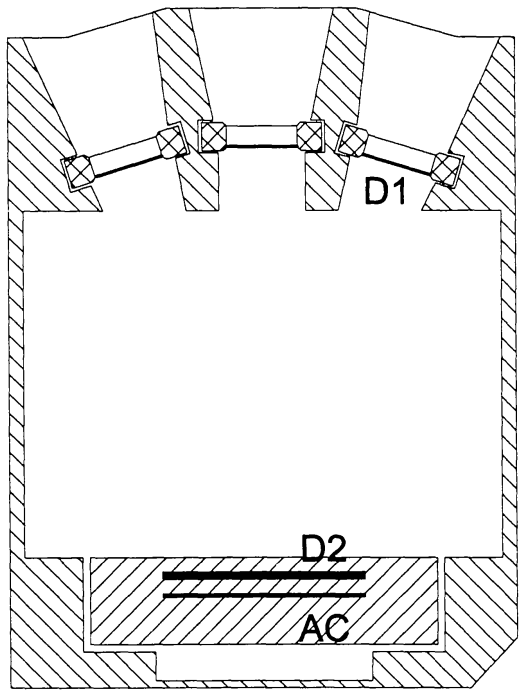

Fig. 4. Cross section of the Low Energy Detector.

The first detector layer (D1) is composed of seven individual detectors, one at the center and the other six in a circle around the central detector (see also Figure 1). The central detector is parallel with the second layer (D2), but the other six D1 detectors are tilted at an angle of 16.7 degrees with respect to the central detector plane as seen in Figure 4. The purpose of this design is to minimize the path length variations in individual ΔE detectors, while at the same time achieving a geometric factor as large as possible for the whole sensor. Also, a passive aluminium collimator is used to limit the access of particles from large zenith angles to the sensor.

Two of the seven D1 detectors are surface barrier detectors with a nominal thickness of 20 microns. The telescopes formed by these two thin detectors and D2 is called LED I, and is used for measurements at the lowest end of the ESU energy range. The other five D1 detectors are ion-implanted detectors with a nominal thickness of 80 microns. The telescopes formed by these five thicker D1 detectors and D2 is called LED II. The active area of all

D1 detectors is 100 mm^2. The thickness uniformity of all D1 detectors were measured using a radioactive source technique (Peltonen et al., 1988). The thickness uniformity of the surface barrier detectors used in the flight model was better than 0.72 %, and that of the ion-implanted detectors better than 0.45 %.

Ion-implanted silicon detectors D2 and AC are mounted in a common stainless steel housing. Detector D2 is composed of two chips, both 500 microns thick, mounted back to back (n^+ sides), and thereby electrically connected together to form a 1 mm-thick detector. The active area is 600 mm^2. One identical chip is used as the AC detector. The distance between the lower surface of D2 and upper surface of AC is 2 mm.

All LED detectors are mounted in an aluminium box, which together with the collimator form an integrated housing with miniature coaxial connectors as the electrical interfaces for signals, detector bias voltages, and a thermistor. Above the D1 detectors facing open space, there are 8 micron-thick gold-coated kapton foils for thermal protection and as shields against electrical interference. The metallized surfaces of the foils are on the inside, and they are electrically connected to the structure of the housing. The distance between the central D1 detector and D2 is 63 mm. The total height of the housing is 98 mm.

3.3.2. High Energy Detector

A schematic cross section of HED is shown in Figure 5. HED consists of altogether six layers of silicon detectors and two layers of scintillators surrounded by an anticoincidence shield. Pulse height measurements are made from all detectors, except from the anticoincidence shield.

The first four layers (S1, S2) are position sensitive strip detectors. Each of the two layers of both S1 and S2 gives the position of incident particles in one dimension. The detectors of each pair are mounted with strips perpendicular to each other. Therefore, the two-dimensional position of incident particles on both S1 and S2 planes can be determined, and the particle trajectory can be reconstructed.

Trajectory information in HED is essential for the path length variations allowed by the large opening angle of HED. Path length variation due to angle of incidence is applied for all ΔE detectors in the pulse height analysis. In addition, the path length of a particle in silicon, and thereby the amount of energy loss, is affected by thickness variations of a single detector. Trajectory information, together with detailed thickness maps of all the silicon detectors, are applied to overcome this source of inaccuracy in heavy isotope analysis on ground.

The large field of view also provides the possibility for anisotropy measurements of the particle flux. Measuring the pitch angle distribution of solar

particles is another important application of the trajectory information from HED.

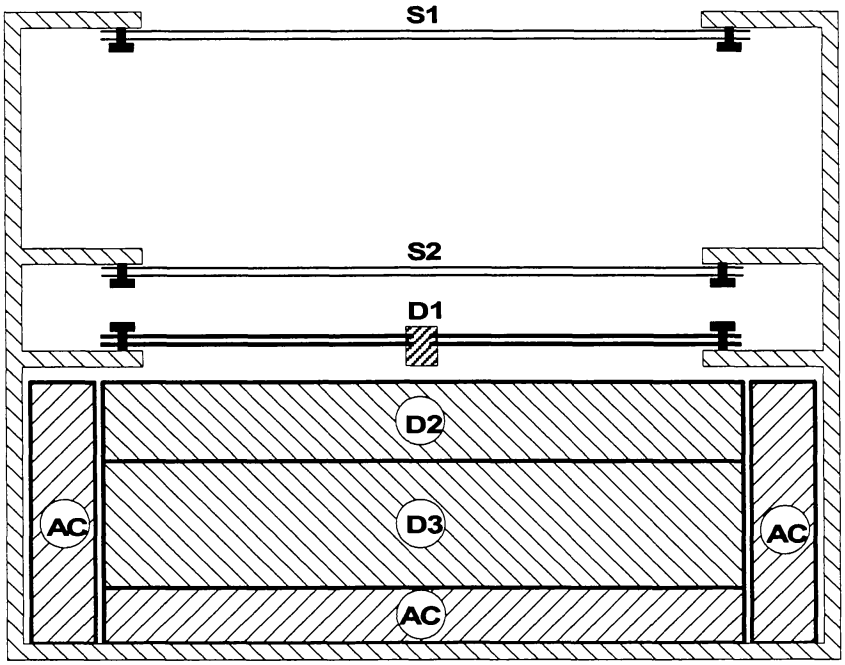

Fig. 5. Cross section of the High Energy Detector.

The active area of one strip detector is 70 x 33 mm^2. Two such chips are mounted side by side with a 4 mm wide inactive area in between, thus giving the outer dimensions of 70 x 70 mm^2 for each of the four S1, S2 layers. The nominally 300 microns thick n-type silicon substrate is cut at a 7° tilt angle with respect to the <111> crystal orientation. The bulk resistivity of the substrate material is between 7000 and 15000 Ωcm. Using a 120 keV phosphorus ion beam, 33 p^+ type strips have been implanted on the top surface of the substrate. The strip size is 70 x 0.9 mm^2 and the strip pitch is 1.0 mm. A schematic cross section showing the structure of the detector is presented in Figure 6a.

A capacitive read-out technique, minimizing the number of required amplifier channels, is applied. As seen in Figure 6a, each p^+ strip is in ohmic contact with an aluminium strip, which is further capacitively coupled to the neighbouring p^+ strip. The coupling capacitance C_{is} was designed to be between 12 and 14 nF. When a reverse bias voltage of -50 V is applied between the strips and the aluminized bottom surface, the detector will be fully depleted. The junction capacitance C_s of each strip is about 20 pF. The equivalent circuit of the detector is a capacitance chain illustrated in Figure 6b. Read-out of the charge pulses caused by particles losing energy in the silicon is made from the two edges of the detector. C_{end} represents the capacitance of the read-out electronics.

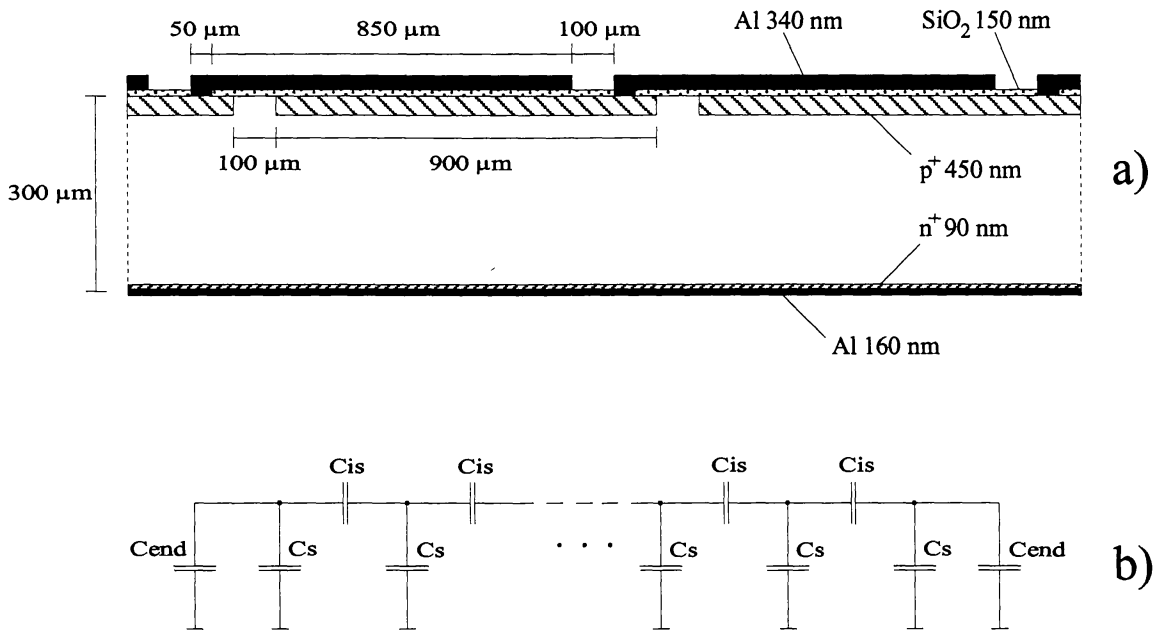

Fig. 6. Schematic drawing of the HED strip detector structure (a) and the equivalent circuit of the strip detector (b).

When an ionizing particle traverses the detector, the generated charge carriers are collected by the strip on top and by the bottom surface because of the applied electric field. The charge from the strip will immediately be distributed through the capacitive chain towards the two edges of the chain, where the read-out by charge sensitive preamplifiers takes place. The ratio of the two charge pulses gives the position of the incident particle. An accuracy equal to the strip width is easily achieved. When the position and the total amount of the charge collected are known, the total energy loss in the detector can be calculated.

As the charge advances in the capacitance chain of Figure 6b, part of it is left into the other strip capacitances. Therefore, the further the charge has to travel, the less will be left at the edge of the chain to be read out. This attenuation causes some nonlinearity in the determination of position, but a simple correction can be applied even in the on-board data analysis. For best accuracy, it is essential to know the charge division in each individual strip detector. Therefore, extensive calibrations of the flight detectors have been carried out at various accelerator facilities, and methods applicable for in-flight data calibration have been developed.

In addition to the strip detectors, conventional ion-implanted silicon detectors are also used for energy measurements in HED. Detector D1 consists

of altogether eight silicon chips with active dimensions of 36 x 36 mm^2 and thickness of 500 microns. These chips are mounted in four quadrants in two layers below the S2 detector (see Figure 5). Due to the limitations in available amplifier channels, four quadrants, two chips in the upper layer and the two chips below these in the lower layer, are electrically connected. Thereby, two independent detectors with an active area of 72 x 36 mm^2 and thickness 1 mm are formed with a 3 mm wide inactive area in between the halves, similar to the strip detectors.

In order to extend the energy range of HED up to hundreds of MeV/n, two layers of scintillators are employed in the bottom part of HED. The first one, D2, is a 7.9 mm thick CsI(Tl) crystal and the second one, D3, is a 14.8 mm thick BGO. Photodiodes on all four sides of the CsI(Tl) crystal are used to collect the light produced by ionizing particles in the scintillator. The number of phodiodes used is 8 and the total active light collecting area about 8 cm^2. Detector D3 consists of five parallel BGO bars with a cross section of 14.8 x 15.2 mm^2. Light is collected from both ends of each bar, with a total light collecting area of 10 cm^2. The area of both D2 and D3 is about 80 x 80 mm^2.

Scintillators D2 and D3 are surrounded by an anticoincidence shield. The shield consists of two independent parts, bottom part AC1 and the four sides AC2. A special plastic scintillator emitting in the wavelength region suitable for photodiode read-out is used. Eight diodes are used to collect the light from each of the two parts AC1 and AC2 of the shield.

As for LED, all HED detectors are mounted in an aluminium box, with similar electrical interfaces for signals, detector bias voltages, and a thermistor using miniature coaxial connectors. Above the S1 detector, there are two metallized plastic foils. The inner foil is aluminized 130 microns kapton with the aluminium surface towards the detectors and electrically connected to the housing. The upper foil is gold coated 80 microns kapton with kapton on the outside facing open space. The distance between the lower surface of S1 and the upper surface of S2 is 29 mm. The equivalent distance between S2 and D1 is 5.5 mm. The distance between the layers giving x- and y-coordinates in S1 and S2 is 1 mm. The total height of the HED housing is 81 mm.

3.4. ESU ELECTRONICS

The ESU electronics is contained in the same instrument box as the sensor housings. The analog interface from the sensors to the amplifier boards is via short coaxial cables. The power from the LVPC to the ESU is connected through a power switching unit (SWU), one of the printed circuit boards of ESU. All ESU supply voltages excluding the power of the data processing unit (DPU) can be switched on and off by the SWU under the control of the DPU. DPU voltage is controlled by the CDPU. The data and timing signals

of the electrical interface described in Section 3.1. are connected to the data processing unit. ESU data and power interfaces are presented in Figure 7.

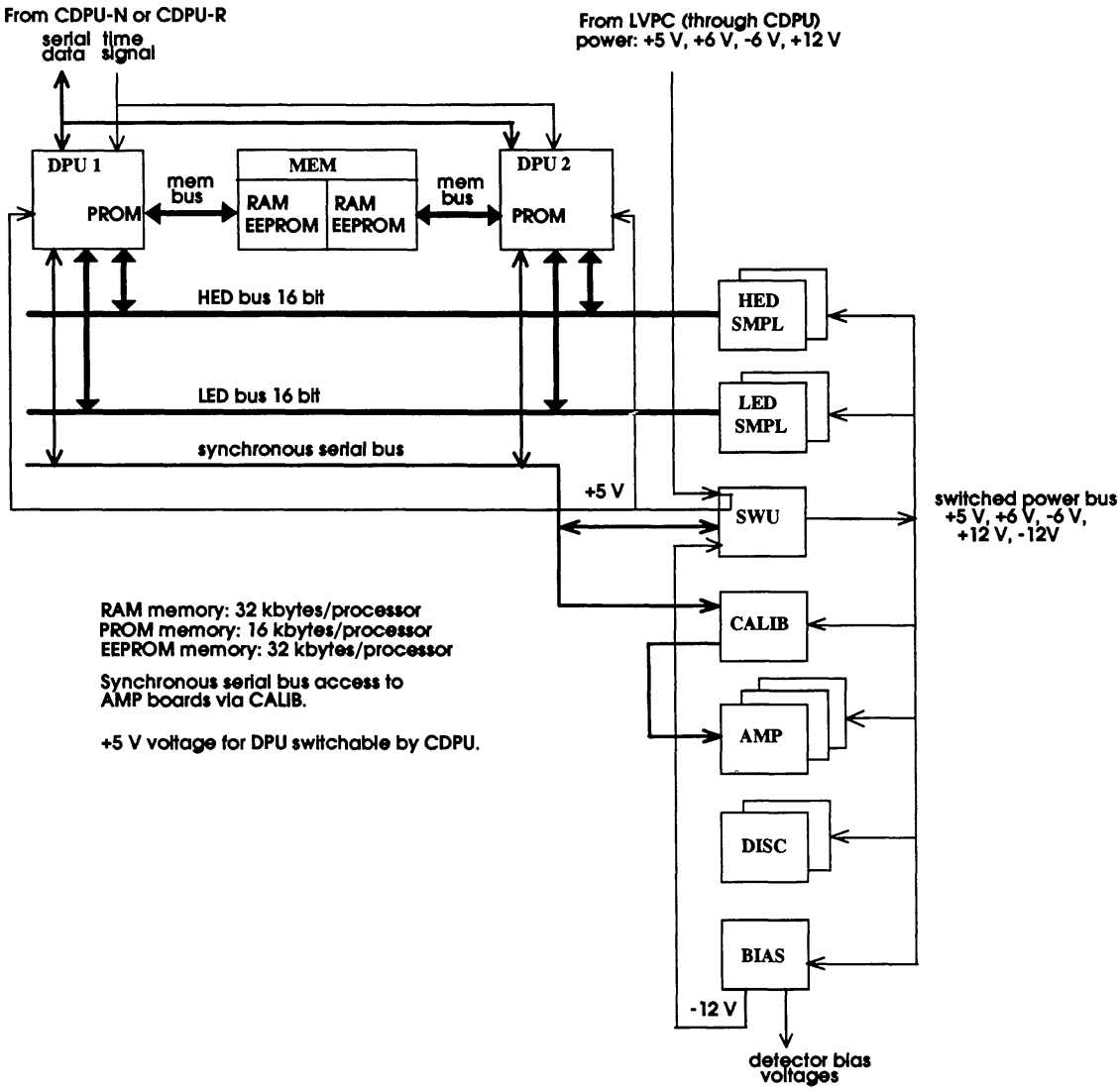

Fig. 7. ESU data and power interfaces.

The ESU electronics consists of 15 printed circuit boards on a mother-board. Most essential parts are doubled and used as cold redundant. This includes the DPU, signal sampling, multiplexing and AD-conversion circuits, and logic, which is realized using gate arrays.

A simplified block diagram of the electronics is presented in Figure 8. The operation of ESU is controlled by the DPU. The main tasks of the DPU are to control the instrument by executing uplinked telecommands, to collect and analyze science data, to collect housekeeping data, and to format

and compress the data before transmitting it to the CEPAC CDPU once a minute. Due to the flexible power switching concept and programmability of the gate array logic, the ESU hardware can be reconfigured efficiently under the control of the DPU. In addition, software controlling the temperature of ESU is always running continuously when the DPU is powered.

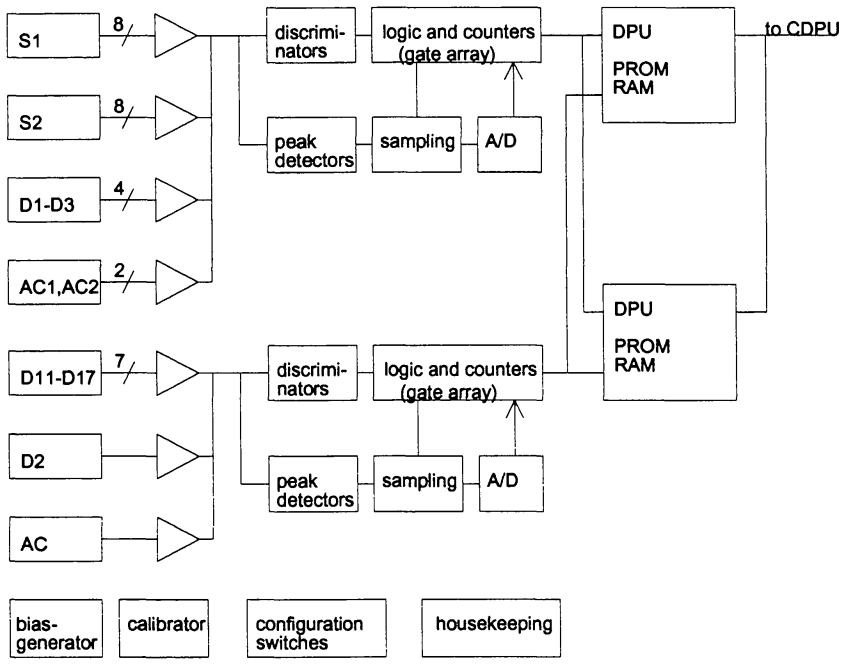

Fig. 8. Simplified block diagram of the ESU electronics.

The HED analog electronics consists of 22 charge sensitive preamplifier channels on two amplifier boards, as indicated in Figure 9. Twenty of these are equipped with further amplification circuits and are viable for pulse height analysis. The remaining two (AC1 and AC2) are used as inputs to discriminator circuits only. Due to the large dynamic range (20000:1) required for covering the HED energy range and ion species, triple gain shaping amplifiers (high, medium and low gain) are used for all signals to be pulse height analyzed. In addition, two shaping times are applied. The rise times are 1.5 μs and 7 μs for fast and slow signals, respectively. Signals amplified with a slow shaping time are selected for AD-conversion by multiplexing circuits. The pulse height of each selected signal is stored in a peak detector (PD) and then converted into digital form by a 12-bit analog-to-digital converter (A/D). All these functions are on HED-SMPL boards, as shown in Figure 9. The multiplexers, peak detectors and the AD-converter are controlled by fast signals derived from the same original charge pulses as the slow signals.

At the heart of the event selection and control of signal multiplexing is the gate array. One gate array was designed for the project, applicable for both HED and LED sensor electronics. The fast signals from the amplifiers are

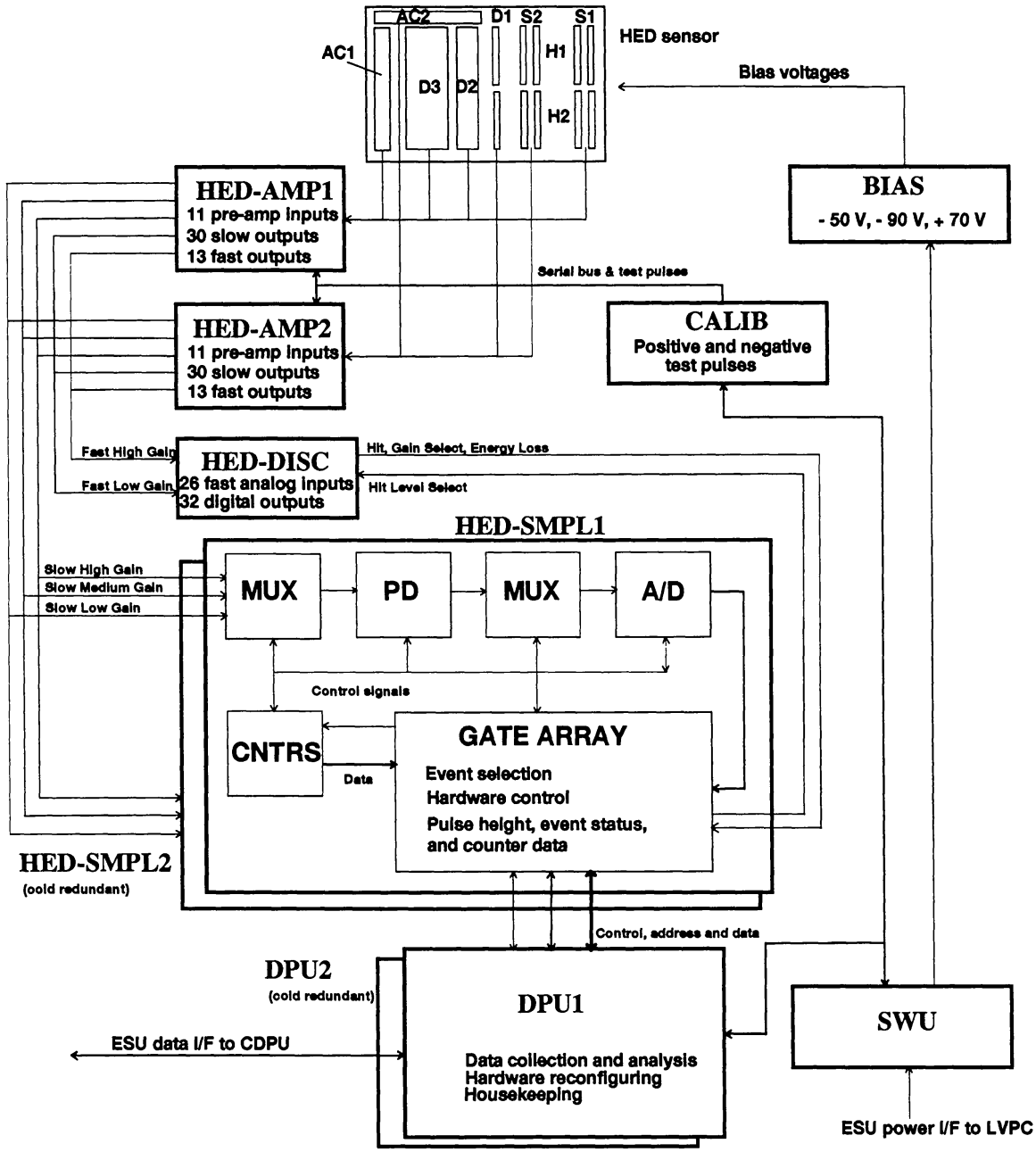

Fig. 9. Block diagram of the HED electronics.

fed into discriminator circuits (HED-DISC) providing outputs corresponding to various levels of energy deposition in individual detectors or to levels of summed signals from a group of detectors. Discriminator logic outputs are used as inputs for the gate array, signifying either excess of the detection threshold in some detectors (Hit signal in Figure 9), a sufficient amount of

energy loss to entail selection of the medium or low gain amplifier channel for analysis (Gain Select), or a signal to be used by the counter logics (Energy Loss) (Figure 9). Inputs of the first two categories are used for controlling the multiplexers in such a way that signals from those detectors through which particles have passed will be selected with appropriate gain. Inputs to the counter logic (CNTRS) are used for incrementing one or more of the sixteen counters used for recording fluxes of various particle species in selected energy ranges.

The gate array determines valid events. The basic requirement for a valid event is that the particle reaches the lower layer of S2, in which case the trajectory can be found. When a valid event is detected, the gate array starts a sampling sequence. For each HED event, 11 signals are selected for pulse height analysis. Of these, eight originate from the strip detectors S1 and S2, and one each from D1, D2 and D3. Events with simultaneous signals from both halves of S1, S2 or D1 are rejected by the logic. At the end of an AD-conversion cycle, the DPU reads the pulse height results with some additional status information characterizing the event.

Capabilities of the gate array have been utilized in improving the fault tolerance of the sensor electronics or isolating misbehaving detectors. The main features in this respect are that each detector can be disconnected from the discriminator inputs and that the corresponding discriminator output can be set either to logic 1 or logic 0. In this way, a noisy detector can be isolated, and still the event condition can be artificially generated. Another feature is that in case of increased noise levels, the threshold of the event condition can be raised to three times nominal (Hit Level Select), thereby avoiding an excessive event rate.

An important property of the gate array is the priority system. HED has a three-level priority system, guaranteeing that in spite of a high rate of protons, the rare particle events that are the most important are recorded. This is achieved by using a software-controlled event rate divider. If the rate of low priority particles rises above a pre-selected level, the software informs the gate array, which in turn allows only a fraction of these low priority events to be analyzed. For low energy protons, the maximum value of the event rate divider is 128.

The structure and functions of the LED electronics are very similar to those of HED. The structure is somewhat simpler due to the smaller number of detectors and generally a much narrower dynamic range. Only the LED D2 detector has three gain ranges, whereas the D1 detectors have only two. The same gate array is used as for HED, but in a different mode. Similar functions are provided for multiplexing signals. LED has only eight counter channels and a two-level priority system.

In addition to the analog and digital electronics and the DPU described above, there are two other important boards closely related to the operation

of the sensors. These are the bias voltage supplies (BIAS) and the in-flight calibrator (CALIB). Both LED and HED need three different bias voltages. For LED these are +15 V and +50 V for the D1 detectors and +90 V for D2 and AC. For HED bias voltages of -50 V are used for the strip detectors, -90 V for the D1 detector, and +70 V for all photodiodes. On the bias board, -12 V voltage is also produced for some circuits, notably the AD-converters. All bias generators and DC/DC converters are redundant. The bias voltages generated by the redundant circuits are 20 % higher than the nominal ones.

The in-flight calibrator provides the means to check the linearity and gain stability of the amplifier chains as well as the discriminator thresholds during the flight. Calibration is made regularly once per month. The nominal calibration sequence is automatic, the routing of pulse injection and pulse heights being controlled by the DPU software and a pre-loaded calibration table. Pulse heights are determined under the control of the DPU by an 8-bit DAC and nominal pulse attenuations of 1, 12, or 144, which gives sufficient accuracy and dynamic range to cover all amplifier channels and gains.

3.5. Particle identification

Particle identification is based on the conventional $\Delta E - E$ technique. The identification of the hydrogen and helium ions is done by a particle identification function in the on-board analysis program (Lumme, 1995). In the on-board analysis the first step is to determine the total energy E and the residual energy E_r, i.e., the energy in the detector layer where the particle has stopped. The preliminary particle identification is given by the formula $P = (E^\alpha - E_r^\alpha)/L$ where L is the thickness of the ΔE detector (or stack of detectors) and $\alpha = 1.7$ is constant. The number P is further processed to give charge and mass of the particle.

At LED energies the PC version of the TRIM package have been used (see Ziegler et al., 1985) and at HED energies the VAX/VMS software developed by Hubert et al. (1990) has been implemented to our Sun/UNIX platform.

Identification of heavier elements is not done by the on-board software. This analysis employs more sophisticated methods based on comparison of the particle energy dissipation in the telescope layers with the theoretically determined energy losses. The fine-calibration of the instrument is done simultaneously with the analysis in order to ensure that the eventual changes in the amplifiers and the detectors are taken into account.

For LED, where only two detector layers are used to determine the particle type and energy, the analysis is straightforward. The total energy E, the Residual energy E_r and the ratio $R = E_r/E$ are determined. R is typically within the range 0.6 ... 0.9. A Particle Identification Number (PIN) is then determined by interpolation based on a table where R and E are theoretically calculated for all ions ($Z = 1 - 30$) with $A = 2Z$. This way the PIN is roughly defined by the relation PIN $= Z + 0.12(A - 2Z)$, which gives, e.g.,

for ^{13}C PIN = 6.12. However, a small post processing is required to correct for the energy and ion dependence of the interpolation. The table needed in interpolation is detector specific, and each D1 window together with the D2 layer has an own table based on the actually measured thickness of that D1 layer.

For HED, the method is basically the same, but because energy dissipation in more than two detector layers is measured, the calibration and analysis takes advantage of this more detailed information. Theoretical energy dissipation patterns have been determined for particles stopping in different layers of HED. These patterns describe the general behaviour which is based on increasing stopping power as the particle decelerates – and finally stops – in the detector layers. In calibration, a sample of particle events is compared with these patterns to adjust the amplification coefficients, and in analysis, these patterns are used to remove events not matching (due to errors or due to heavy straggling) in order to improve the resolution. The final determination of the PIN is done as described for LED.

3.6. On-board software

The ESU DPU is a (MIL-STD-1750A) MAS281 with a clock frequency of 19.6608 MHz. The on-board software consists of a specifically designed preemptive real-time kernel together with associated user processes. The real-time kernel provides the usual operating system services. User processes take care of the main ESU activities: on-board analysis of LED and HED events, housekeeping, communication with the CEPAC CDPU, thermal control of the instrument, and calibration of LED and HED.

From scientific point of view, the most important task of the DPU is the on-board handling of the particle events. Only H and He ions and electrons are analyzed on-board; data of elements heavier than ^{4}He are transferred to ground as pulse heights, and these data are used both to identify the particles and to calibrate the instrument. The program has only one measurement mode, which is able to run in both low and high particle flux. During high flux, the heavy elements are given higher priority and only samples of H and He ions are analyzed.

Recording of HED and LED events is performed at three levels. At the first level, various hardware counters are updated. The counter upkeep is handled by the gate array logic with no processor involvement. Among other things, these counters provide the primary measurement of the ambient flux. The next level is the interrupt service software module of the DPU, which is rewoken at each event accepted by the gate array. Besides reading the AD-conversion results for further analysis, it also monitors the load of the analysis module. In order to adapt to the varying flux, the interrupt rate from the low energy protons can be adjusted using the gate array's event rate dividers. The third level is the eventual event analysis. The lightest and

most abundant isotopes up to ^{4}He are identified, and energy-mass intensity tables are updated accordingly. Proton intensities in each energy channel are also recorded using 10-second time resolution.

For HED, the direction of incident protons and ^{4}He are also recorded for anisotropy measurements using an integration time of four minutes. Proton directions are recorded in three energy bands (12.5-16, 20-25 and 50.5-160 MeV/n) and ^{4}He in two bands (12.5-20 and 40-160 MeV/n). The directional distributions are recorded as two mutually perpendicular one-dimensional intensity profiles with 2° resolution.

In addition to nuclei, HED also detects electrons, which are recorded according to the penetration depth (D2 or D3) and pulse height in the stopping detector. There are 10 and 6 counting channels for electrons stopped in D2 and D3, respectively. A major part of the total telemetry is reserved for the heavy ion events ($Z > 2$) which are transferred as packed pulse heights for detailed analysis on ground.

The primary integration period for the measurements is 59.95312 seconds (anisotropy measurements utilize 4 times longer time), corresponding to a fixed-size data packet of 5756 bytes. According to bench tests, the analysis capacity is expected to be between 2000-2500 analyzed HED and LED events per second, depending on the ambient flux. When the flux rises, the gate array logic is used to decrease the relative amount of protons (and eventually He ions) to be analyzed in order not to miss any heavy ions event.

4. Scientific Performance

In ERNE, special emphasis has been put on isotopic resolution both in instrument design as well as in the development of the on-board data acquisition software and the methods of data analysis on ground. From the theoretical point of view it is clear that the isotopic resolution varies with particle type and energy. The general goal has been to resolve isotopes up to Ne in LED and up to Fe in HED.

Below are presented results from Flight Model accelerator tests at SARA in Grenoble in October 1993. A total of 11 test runs were carried out using a 27.9 MeV/n ^{58}Ni primary beam together with various targets (Co, Au, Al, C). The purpose of these accelerator tests was to verify the overall performance of the ERNE Flight Model as well as to do the calibration of the instrument.

4.1. LED

The LED electronics is a relatively simple construction with two amplifier gain ranges in D1 and three in D2. Calibration of these amplifiers includes determination of offsets and linear coefficients.

A PIN histogram describing the mass resolution is shown in Figure 10. The mass resolution of each element was calculated assuming a Gaussian distribution. The resolution of, e.g., carbon isotopes is $\sigma_m = 0.22$ amu and that of neon isotopes is $\sigma_m = 0.30$ amu. In another accelerator test at GANIL in August 1993 where fixed rigidity ions were used the resolution was slightly better, but this can be explained by the very narrow energy range of each isotope in that test. The two accelerator tests clearly show that resolution of neon isotopes is achieved.

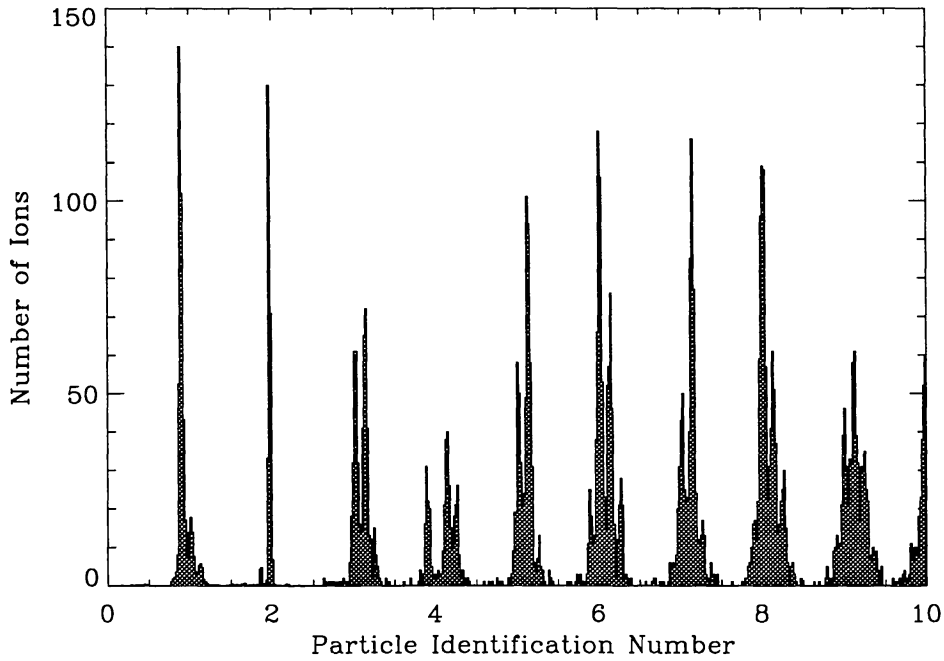

Fig. 10. Particle Identification Number histogram in a LED accelerator test.

4.2. HED

In HED, the particle penetrates through several detector layers before it stops. The energy dissipation in each layer is compared with a typical behavior of a particle where the stopping power increases with decreasing energy. The events which do not fit into this scheme due to straggling or errors in pulse height can be rejected, and this can be used to improve the isotopic resolution. Figure 11 gives a sample of data in one of the accelerator runs.

Isotopic resolution varies with particle type and energy; The highest resolution is achieved at medium energies of HED (a few tens of MeV/n). In Figure 11 the mass resolution of carbon is $\sigma_m = 0.17$ amu. The resolution was further increased by rejecting the events where the error in pulse height in any of the detector layers was greater than 7 %. In that case 9 % of event were rejected and the resolution of carbon was $\sigma_m = 0.15$ amu. In

the accelerator test in GANIL where heavier elements were present in the beam the resolution for silicon was determined by this method to be $\sigma_m = 0.20$ amu. Although no definite conclusions about isotopic resolution of Fe can be drawn from the results above, it can generally be stated that the instrument performance shows good agreement with the design goals and that HED seems to fulfill the requirements set by the scientific motivation of the experiment.

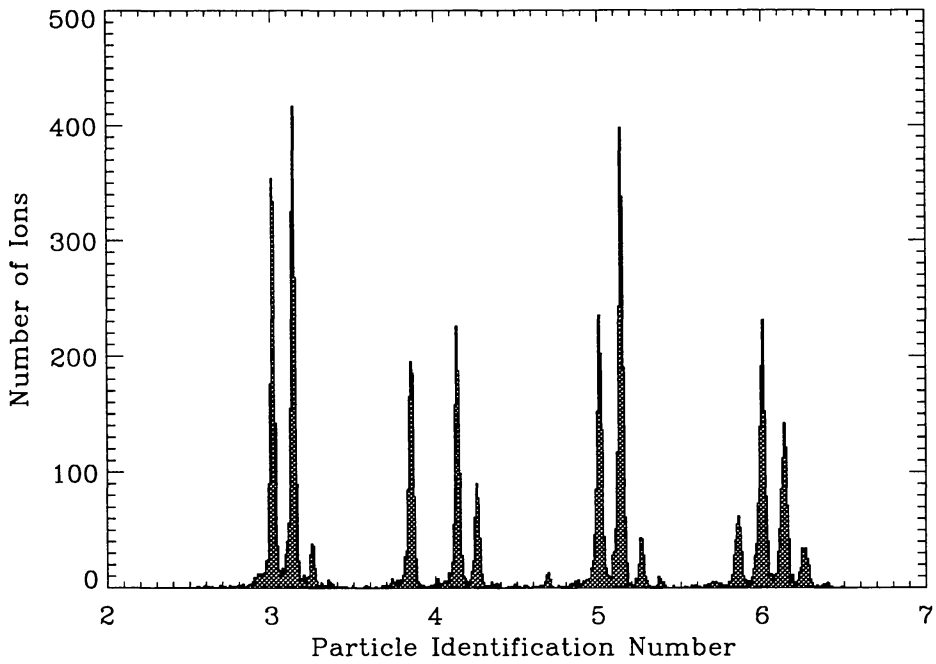

Fig. 11. Particle Identification Number histogram in a HED accelerator test.

4.3. Electrons

One of the scientific objectives of ERNE is to determine the energy spectrum of interplanetary electrons in the MeV range. HED is designed to detect relativistic electrons, nominally in the energy range 2 - 50 MeV.

As a highly relativistic electron traverses the detector medium, the main energy loss mechanisms are ionization and bremsstrahlung. Since high energy radiation quanta may escape the detector without noticeably interacting in the detector, the pulse height spectra of monoenergetic electrons become relatively broad. Furthermore, collisions with the electrons of the medium may result in considerable straggling in the trajectory of the incident electron. This also decreases the measurement accuracy of a single electron event.

Due to the facts described above, the electron data analysis has to be based on the statistical analysis of a sample electron population. The essence

of the data analysis lies in the good knowledge of the detector performance in electron measurements. Therefore, special emphasis was put in the pre-launch studies of the detector and in developing good theoretical models.

Using calibration measurements with accelerated electrons and extensive computer simulations, various properties of HED related to electron measurements have been determined. Figure 12 shows the measured and simulated D2 and D3 response functions for 30 MeV electrons. Generally, the measured distributions are a little broader than the simulated ones indicating that all characteristics of the detector-photodiode system are not fully taken into account in the simulations. Specifically, the measured D3 values exceeding 30 MeV originate from events occurring in the immediate vicinity of the photodiodes. The detection of light pulses from such events is significantly more efficient than that from events taking place in the middle of the scintillator block.

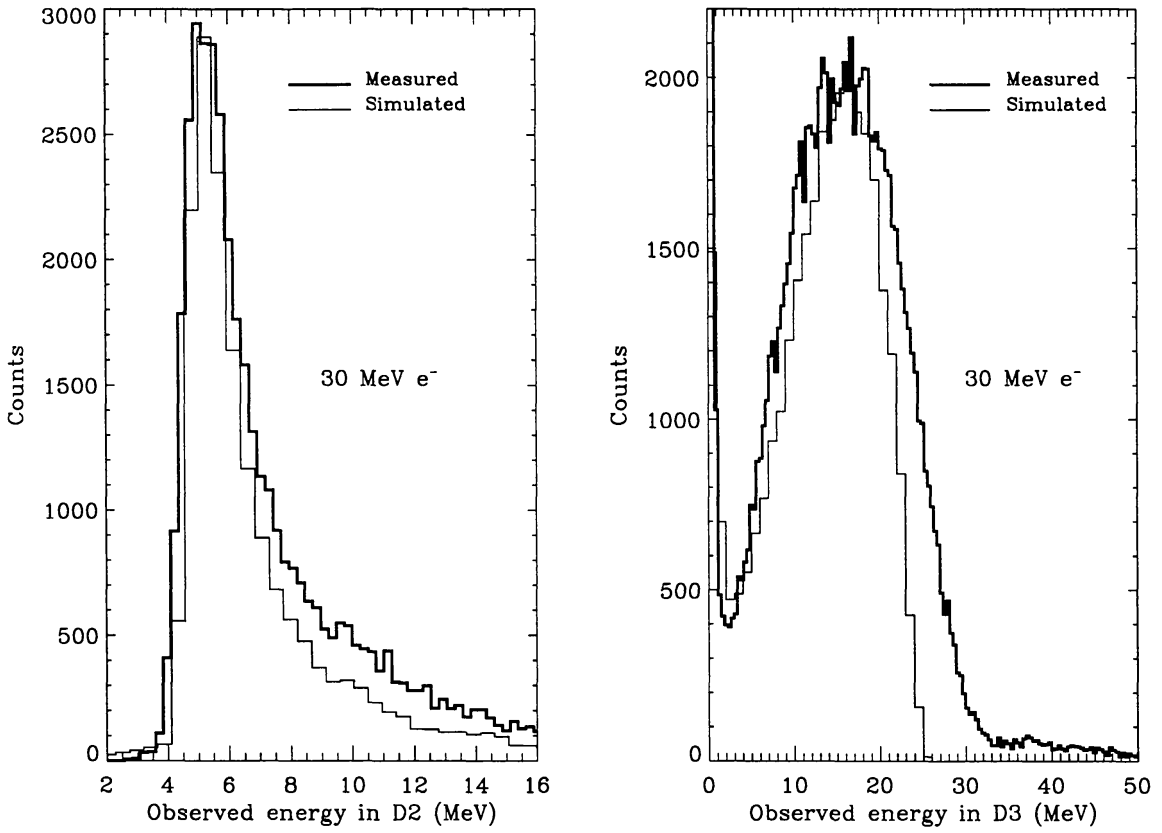

Fig. 12. Measured and simulated response functions of the ERNE HED D2 and D3 detectors to 30 MeV electrons arriving perpendicularly at the detector.

The computer simulations are based on the GEANT 3 code. These simulations provide us with the theoretical energy loss data, whereas the test results represent the real detector response. To explain the differences between calculations and measurements, supplementary models are being developed.

The simulations, .e.g., take into account the transport of light in the HED scintillation detectors. Combining these new models with the GEANT code gives us a powerful tool for the performance studies of the detector, and thereby a better understanding of the measured response.

4.4. Comparison with other satellites

A comparison between ERNE on the three-axis stabilized SOHO satellite and other space-born particle experiments of the 1990's might include the following spinning (or earth-orbit) satellites. The ACE and WIND satellites have instruments that measure the same energy range as ERNE, and they will also eventually end up at the same place in space, the Earth-Sun L1 point. The ACE satellite is purely a particle observatory carrying high energy particle detectors CRIS and SIS,and a magnetometer (IACG, 1994). The WIND mission has also a high energy particle detector EPACT (Barbier et al., 1993).

The SAMPEX mission on a polar Earth orbit has several particle detectors, and the energy ranges in the high energy region are comparable to those of ERNE. The MAST instrument (Cook et al., 1993) is similar to HED, but with lower geometric factor. The Geotail mission focusing on the Earth's magnetotail carries the HEP particle detectors (Doke et al., 1989) comparable to those of ERNE.

The Ulysses satellite on an orbit inclined to the ecliptic has a magnetometer and the particle instrument COSPIN (Simpson et al., 1992), with special emphasis on the modulation of galactic cosmic rays in the polar regions of the Sun.

5. Ground System Facilities and Data Analysis Scenario

For the pre-flight tests at unit and system levels, an electrical ground support equipment (EGSE) was developed. Both CEPAC common and ERNE specific systems were produced. The complete CEPAC EGSE consists of four computers, one of which is used as interface to the ESA and NASA provided test facilities (CCS and ECS). The interface to the CCS is a computer (CEGSE, i.e. Common Electrical Ground Support Equipment), which disassembles the TCP data flow containing CEPAC data packets as acquired from the on-board CEPAC experiment and redirects the instrument data to the appropriate experimenter's GSE systems. Each sensor unit within CEPAC has one sensor EGSE, which is used to analyze the housekeeping and science data.

The CEGSE is a stand-alone system, capable to some extent of verifying the functionality of the whole CEPAC experiment without the presence of the sensor EGSE's. Validity of the data flow and certain housekeeping parameters can be monitored in real time. The telemetry flow is

archived onto CEGSE's backup media in real time, and the sensor EGSE's can retrieve the data later for processing and analysis.

The ESU SEGSE is capable of presenting science data in real-time on a graphics display. The science data are presented as pulse height distributions of each detector. The data can be viewed also in text mode, which allows simultaneous monitoring of ESU housekeeping and science data as well as the housekeeping data of the LVPC.

During flight, the fluxes of energetic particles are monitored from the particle data display window of SEGSE. Real time and tape dumps of proton and ^{4}He count rates in a few selected energy channels and electron count rates are plotted as a function of time. This also allows the user to monitor the functioning of the sensors and the on-board science software.

In the SEGSE software display window are shown various flags, status parameters and monitoring counters. Further, the functioning of the gate array and the on-board anisotropy analysis software is verified in this window.

The analysis of the instrument data is done in three different environments. The data processing in the on-board processor gives as output the flux of hydrogen and helium isotopes and the "raw data" of heavier elements. Also the anisotropy of the flux in a few selected channels is measured and compressed into two one-dimensional profiles.

The second data processing environment is the NASA CDHF where the proton and helium data is further analysed to give the flux in various channels. Also isotopic abundance ratios of H and He are determined. This is done daily by the CDHF staff, and as the output the ERNE Key Parameters are obtained. The Key Parameters are available both on-line at CDHF and merged into the SOHO Summary Data. Further, the Key Parameters are distributed by the NASA DDF on CD-rom disks to the solar physics community.

The most detailed analysis is done at the PI home institute where the work is done using Unix-workstations. In addition to a number of instrument specific programs needed in both calibration and identification of the particles, we also use most of the software packages which have been commonly agreed to be used within the SOHO community.

When particles have been identified, we will have a database describing the flux of all elements from H to Ni and a number of isotopic abundance ratios as a function of time. This is the base for the scientific analysis, and it is used to produce spectra and time-profiles during SEP events.

A separate analysis line is used for determining the particle flux anisotropy. The data have been compressed by the on-board analysis software, and these data together with the instrument directional response function is used in determining the pitch angle distribution.

Acknowledgements

The Technology Development Centre and the Academy of Finland are thanked for financial support.

References

Barbier, L. M., Reames, D. V., and von Rosenvinge, T. T.: 1993, *Vol. 3* **Proceedings of the 23rd International Cosmic Ray Conference**, 222.

Cook, W.R., Cummings, A. C., Cummings, J. R., Garrard, T. L., Kecman, B., Mewaldt, R. A., Selesnick, R. S., Stone, E.C., and von Rosenvinge, T. T.: 1993, *IEEE Transactions on Geoscience and Remote Sensing* **31**, 557.

Doke, T., Kikuchi, J., Nishijima, K., Hasebe, N., Murakami, H., Nakamoto, A., Yanagimachi, T., Ito, K., Kohno, T., Nagata, K., Wilken, B., Maezawa, K., Terasawa, T., Yanagita, S., and Nishida, A.: 1989, *The Institute of Space and Astronautical Science* **Report No. 10**.

Forman, M.A., Ramaty, R., and Zweibel, E.G.: 1986, 'Chap. 13' in P. A. Sturrock, T. E. Holzer, D. A. Mihalas, and R. K. Ulrich, ed(s)., *The Physics of the Sun, vol. II*, D. Reidel Publ. Co.: Dordrecht, Holland, 249.

Gosling, J. T.: 1993, *JGR* **98**, 18937.

Hubert, F., Bimbot, R. and Gauvin, H.: 1990, *Atomic Data and Nuclear Tables* **46**, No. 1.

Inter-Agency Consultative Group for Space Science (IACG): 1994, *Handbook of Missions and Payloads* .

Kunow, H., Wibberenz, G., Green, G., Mueller-Mellin, R., and Kallenrode, M-B.: 1991, 'Chap. 11' in R. Schwenn and E. Marsch, ed(s)., *Physics of the Inner Heliosphere 2*, Springer-Verlag: Berlin Heidelberg, Germany, 243.

Lumme, M.: 1995, *Ph.D. thesis, Department of Physics, University of Turku*, Data Analysis of the Energetic Particle Experiment On-Board the SOHO Satellite.

Müller-Mellin, R., Kunow, H., Fleissner, V., Pehlke, E., Rode, E., Röschmann, N., Scharmberg, C., Sierks, H., Rusznyak, P., McKenna-Lawlor, S., Elendt, I., Sequeiros, J., Meziat, D., Sanchez, S., Del Peral, L., Witte, M., Marsden, R., Henrion, J.: 1995, *this issue of Solar Physics* .

Peltonen, J., Nieminen, A., Sarjala, A.: 1988, *ERNE Internal Report* **51**.

Reames, D. V.: 1995, *Adv. Space Res.* **15**, 41.

Schwenn, R., Marsch, E.: 1990, *Physics of the Inner Heliosphere, vol 1: Large-Scale Phenomena*, Springer-Verlag, 146.

Simpson, J. A., Anglin, J. D., Balogh, A., Bercovitch, M., Bouman, J. M., Budzinski, E. E., Burrows, J. R., Carvell, R., Connell, J. J., Ducros, R., Ferrando, P., Firth, J., Garcia-Munoz, M., Henrion, J., Hynds, R. J., Iwers, B., Jacquet, R., Kunow, H., Lentz, G., Marsden, R. G., McKibben, R. B., Mueller-Mellin, R., Page, D. E., Perkins, M., Raviart, A., Sanderson, T. R., Sierks, H., Treguer, L., Tuzzolino, A. J., Wenzel, K.-P., and Wibberenz, G.: 1992, *Astron. Astrophys. Suppl. Ser.* **92**, 365.

Torsti, J., Vainio, R., Schultz, G., Halén, S.: 1994, *Proc. of the Third SOHO Workshop, Solar Dynamic Phenomena and Solar Wind Consequences* **ESA SP-373**, 117.

Wibberenz, G., Kecskeméty, K., Kunow, H., Somogyi, A., Iwers, B., Logachev, Yu. I., Stolpovskii, V. G.: 1989, *Solar Physics* **124**, 353.

Ziegler, J. F., Biersack, J. P., and Littmark, U.: 1985, *The Stopping and Range of Ions in Solids*, Pergamon Press, New York.